Comparative study of the flexural properties of ABS, PLA and a PLA-wood composite manufactured through fused filament fabrication

J.A. Travieso-Rodriguez and R. Jerez-Mesa
Mechanical Engineering Department, Universitat Politecnica de Catalunya, Barcelona, Spain
Jordi Llumà
Department of Material Science and Metallurgical Engineering, Universitat Politecnica de Catalunya, Barcelona, Spain
Giovanni Gomez-Gras
Department of Industrial Engineering, Institut Quimic de Sarria, Barcelona, Spain, and
Oriol Casadesus
Universitat Politecnica de Catalunya, Barcelona, Spain

Abstract

Purpose – The aim of this paper is to analyze the mechanical properties of acrylonitrile-butadiene-styrene (ABS) parts manufactured through fused filament fabrication and compare these results to analogous ones obtained on polylactic acid (PLA) and PLA–wood specimens to contribute for a wider understanding of the different materials used for additive manufacturing.

Design/methodology/approach – With that aim, an experimental based on an L27 Taguchi array was used to combine the specific parameters taken into account in the study, namely, layer height, nozzle diameter, infill density, orientation and printing velocity. All samples were subjected to a four-point bending test performed according to the ASTM D6272 standard.

Findings – Young's modulus, elastic limit, maximum stress and maximum deformation of every sample were computed and subjected to an ANOVA. Results prove that layer height and nozzle diameter are the most significant factors that affect the mechanical resistance in pieces generated through additive manufacturing and subjected to bending loads, regardless of the material.

Practical implications – The best results were obtained by combining a layer height of 0.1 mm and a nozzle diameter of 0.6 mm. The comparison of materials evidenced that PLA and its composite version reinforced with wood particles present more rigidity than ABS, whereas the latter can experience further deflection before break.

Originality/value – This study is of interest for manufacturers that want to decide which is the best material to be applied for their application, as it derives in a practical technical recommendation of the best parameters that should be selected to treat the material during the fused filament fabrication process.

Keywords Fused deposition modeling, Stress (materials), Composite materials, PLA, ABS, Flexural properties

Paper type Research paper

1. Introduction

Additive manufacturing (AM) is a set of techniques with which a part is manufactured by a material stacking technique (Gibson *et al.*, 2010). AM methods are also known as 3D printing, paying a tribute to the techniques that decades ago allowed obtaining of flat shapes from digital files on paper or other surfaces. The concept of 3D printing has now been fully introduced to society. It is far from being an unknown technology because there has been a huge expansion of RepRap devices based on the fused filament fabrication (FFF) principle (Pîrjan and Petroşanu, 2013). The technological advances in these devices and the higher accessibility to them have allowed its introduction in low-scale manufacturing contexts, where it is not only used for prototyping, but to manufacture final parts (Wohlers, 2016). It is therefore important for this technology to be characterized in detail from all points of view (Jerez-Mesa *et al.*, 2018).

Although AM techniques have progressed greatly, many challenges must still be addressed, especially when referring to low RepRap machines (Guo and Leu, 2013). These are usually used in local scale environments, and are often designed as open source devices, what allows users to modify and custom the manufacturing routine by varying numerous parameters to

The current issue and full text archive of this journal is available on Emerald Insight at: **https://www.emerald.com/insight/1355-2546.htm**

Rapid Prototyping Journal

[ISSN 1355-2546]
[DOI 10.1108/RPJ-01-2020-0022]

Received 29 January 2020
Revised 11 June 2020
Accepted 23 September 2020

generate the GCODE. In this sense, one of the main vectors of innovation is the assessment of mechanical properties of parts manufactured through FFF, which are complicated to predict because they are the consequence of an extensive parameter set defined prior to the manufacturing process. Sood *et al.* (2012) demonstrated that the relationship between these printing parameters and the response obtained is extremely complex using an experimental design. Furthermore, workpieces are strongly anisotropical, as their mechanical behavior depends heavily on the orientation of the fibers and the stacking direction of the layers (Garg *et al.*, 2017).

In parts obtained by AM, mechanical properties are dependent on hierarchical interactions between the elements that compose them. In the first level, the interlayer cohesion forces between the different layers must be considered (Domingo-Espin *et al.*, 2015). In a second level, these layers are formed by adjacent filaments that have strong bounds, what is called intralayer adhesion. And finally, there is the molecular cohesion of the polymer chains (Gurrala *et al.*, 2014). Of all of them, the first one is the weakest, and are the one to consider in order to understand what is the limiting factor of mechanical strength of an AM part. For this reason, the thermal history of a part has also influence on its mechanical strength and properties. Sood *et al.* (2010), proved that the lower the layer height, the greater number of layers must be deposited and the material is longer exposed to heating, what favors neck growth between layers. Wang *et al.* (2007) concluded that the nozzle diameter also has influence on thermal diffusion, and should be as small as possible to favor that effect, which ultimately increases resistance.

As fibers define that strength, workpieces always have a direction where the mechanical properties are more favorable depending on the external load (Sun *et al.*, 2008). With the same external load, depending on the bearing load type, the resistance depends on a combination of the intra-layer and inter-layer forces (Gurrala and Regalla, 2012). In case of tensile tests, Garg *et al.* (2017) showed that a piece's resistance depends largely on the orientation of the fibers relative to the applied force. When the lead is aligned with the direction in which the fibers are deposited, resistance is enhanced to an extent by which it can be assimilated to analogous pieces made by injection. This was also true when the tensile force is dynamic, as confirmed by Puigoriol-Forcada *et al.* (2018) in fatigue tests run on several different specimens that had different layer stacks. In terms of compression, workpieces fail by buckling, that causes the layers in the same direction of the load to break, unlike those that are deposited perpendicular to the compressive force, that show a higher resistance Bagsik *et al.* (2010).

Another way of enhancing the mechanical performance of workpieces is by choosing the appropriate material to manufacture them. Polymeric materials such as acrylonitrile-butadiene-styrene (ABS) and polylactic acid (PLA) are the most commonly used in low scale FFF processes. Other materials, such as composites and ceramics, are also used for certain applications. To confirm which material is suitable in each case, many authors have worked to characterize the mechanical behavior of each one (Liu *et al.*, 2019). Through different mechanical assessments, such as bending tests (Belouettar *et al.*, 2009), fatigue tests (Gomez-Gras *et al.*, 2018; Domingo-Espin *et al.*, 2018; Travieso-Rodriguez *et al.*, 2020) and tensile tests (Andrzejewska *et al.*, 2019; Peker *et al.*, 2020; Aydin and Kucuk, 2018), an estimation of those properties can be made.

The revision of the bibliography shows that extensive research has been made to understand the mechanical properties of materials for the FFF process. At sight of the discussed state of the art, the main purpose of this article is to offer a comprehensive view of the flexural properties of the three most common materials used for FFF in the same reference, offering the reader an extensive collection of experimental results and thorough comparison of all of them. First of all, the relationship between the mechanical properties and the manufacturing parameters used to generate ABS workpieces was studied in order to determine their best combination using a Taguchi L27 orthogonal array. Then, results are compared to the ones obtained from PLA pieces, and a material composed of PLA and wood fibers (henceforth Timberfill), manufactured under the same conditions and examined by our group in previous studies (Travieso-Rodriguez *et al.*, 2019). By combining the three sets of experimental results, this paper offers an integrated view of bending tests performed according to the ASTM D 6272 standard on three different materials.

The relevance of the results of this paper can serve as a recommendation when parts that will be subjected to bending loads are manufactured. Also, many sources report that ABS could arise health issues, hence the importance of knowing which materials could be eligible to substitute it. The experimental campaigned detailed about the ABS material is justified so that it can be compared to the PLA and PLA–wood composite results, as three result sets based on a L27 Taguchi array shall be available for comparison. This is especially valuable when it comes to selecting which material to use for different applications. Also, no results based on the method described in the ASTM D 6272 standard have been previously found. This paper focuses ultimately on the search for the appropriate manufacturing parameters in order to obtain the best mechanical properties, two aspects that are not covered as a comprehensive comparison between three different materials in most of the papers found in the literature on additive manufacturing.

2. Materials and methods

2.1 Materials used

In this study, three materials were used to manufacture specimens, namely, ABS, PLA and Timberfill, and are to be compared in terms of flexural mechanical properties. All of them are manufactured and provided by the company Fillamentum. These three materials have been chosen for two reasons. The first one is that they are used for the same application field, so it makes sense to understand comparatively how one performs with regards to the other two. Secondly, PLA is the most sold material in the world, and ABS and Timberfill have the same market share in Europe and the USA, according to the manufacturer, thus the relevance of selecting these three materials for the sake of comparison. The characteristics of the materials according to the manufacturer are listed below in Table 1. The process described in the text T1

refers to ABS, but at the end, the results obtained by all three materials will be presented and they will be compared. Particularly, PLA and Timberfill will be fed from previous publications, that include the same experimental designs. (Travieso-Rodriguez *et al.*, 2019; Zandi *et al.*, 2020b)

2.2 Specimens

The specimens were manufactured according to the guidelines included in the ASTM D6272 standard, which also describes how the four-point bending tests must be conducted. They have a prismatic shape and dimensions of 80x10x4 mm [Figure 1(A)]. They were printed on a SIGMA R17 printer from the company BCN3D. To have stabilize the manufacturing conditions, all five specimens for each specimen type were manufactured at the same time. Then they were painted with a spray to obtain an irregular color surface to allow the image obtained during the test analysis [Figure 1(B)] to be processed.

2.3 Experimental design

This study took into consideration the influence of six different variables: nozzle diameter, layer height, infill density, printing velocity, raster orientation and infill pattern. Figure 2 shows the three different raster orientations used in the experimental design and their denominations. For each parameter, three levels were defined, as can be observed in Table 2.

To perform the minimum number of experiments, a Taguchi L27 DOE was applied to combine the factors (Table 3). This array allows the extraction of results regarding the influence of all factors as well as three interactions between the nozzle diameter, layer height and infill density. Each row of the array describes the combination of factors to obtain each type of specimen. For each of them, five identical specimens were tested for each of them, to confirm the repeatability of results. Therefore, the results of 135 trials were tested and evaluated.

The slicing software used to obtain the GCODE to manufacture the specimens offers the possibility of changing many other variables, that were kept constant in this case. For this reason, there are a series of parameters that remain constant. A summary of the most important ones is given in Table 4. The reader can refer to the Slic3r user manual regarding the additional parameters in it. It is worth mentioning that, as there are no standards regulating how additive manufactured specimens should be tested, it was decided that 1.2 mm would be the perimeter width, because this was the least common multiple of the three layer heights that were included in the DOE (0.1, 0.3, 0.4).

Figure 1 (A) Specimen dimensions; (B) Painted specimen to measure its deformation

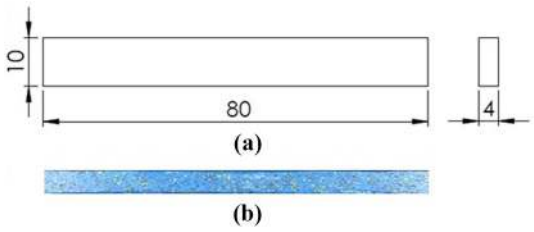

Figure 2 Raster orientation considered in the experimental design

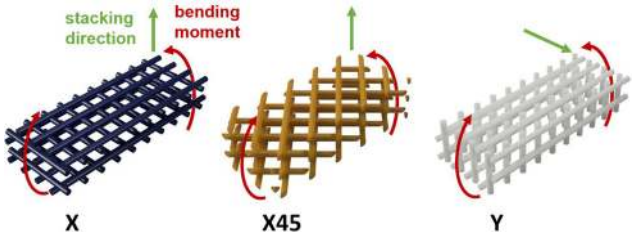

Table 2 Factors and levels used in the study

	Levels		
	Lower	Middle	High
Nozzle diameter (mm)	0.3	0.4	0.6
Layer height (mm)	0.1	0.2	0.3
Infill density (%)	25	50	75
Printing velocity (mm/s)	20	30	40
Orientation	X	Y	X 45°
Infill pattern	Rectilinear	Linear	Honeycomb

2.4 Description of the four-point bending experiment

The specimens were subjected to four-point bending tests for plastic materials as per the ASTM D6272 standard. This method consists of performing a test with a specimen supported on two pairs of lower and upper rollers (Figure 3). This method has proved to deliver reliable results in other parts obtained by AM techniques (Olivier *et al.*, 2016). Figure 2 shows the characteristics of the test.

Table 1 Properties of materials used in this study

Characteristic	ABS Extrafill "Sky Blue	PLA Extrafill "Chocolate Brown	Timberfill
Filament diameter (mm)	2.85 ± 0.05	2.85 ± 0.05	2.85 ± 0.05
Material density (g/cm3)	1.04	1.24	1.26
Tensile Yield Strength (MPa)	39	60	39
Elongation at break (%)	20	6	2
Flexural Strength (MPa)	60	83	Not provided
Flexural modulus (MPa)	1,900	3,800	Not provided
Tensile modulus (MPa)	Not provided	3,600	3,200
Print temperature (oC)	200–240	190–210	150–170
Hot Pad (oC)	80 – 105	50 – 60	50 – 60

Table 3 Experimental design represented by an L27 Taguchi orthogonal array

Run	Nozzle diameter (mm)	Layer height (mm)	Fill density (%)	Printing velocity (mm/s)	Orientation	Infill pattern
1	0.3	0.1	25	20	X	Rectilinear
2	0.3	0.1	50	30	Y	Linear
3	0.3	0.1	75	40	X45°	Honeycomb
4	0.3	0.2	25	30	Y	Rectilinear
5	0.3	0.2	50	40	X45°	Linear
6	0.3	0.2	75	20	X	Honeycomb
7	0.3	0.3	25	40	X45°	Rectilinear
8	0.3	0.3	50	20	X	Linear
9	0.3	0.3	75	30	Y	Honeycomb
10	0.4	0.1	25	30	X45°	Linear
11	0.4	0.1	50	40	X	Honeycomb
12	0.4	0.1	75	20	Y	Rectilinear
13	0.4	0.2	25	40	X	Linear
14	0.4	0.2	50	20	Y	Honeycomb
15	0.4	0.2	75	30	X45°	Rectilinear
16	0.4	0.3	25	20	Y	Linear
17	0.4	0.3	50	30	X45°	Honeycomb
18	0.4	0.3	75	40	X	Rectilinear
19	0.6	0.1	25	40	Y	Honeycomb
20	0.6	0.1	50	20	X45°	Rectilinear
21	0.6	0.1	75	30	X	Linear
22	0.6	0.2	25	20	X45°	Honeycomb
23	0.6	0.2	50	30	X	Rectilinear
24	0.6	0.2	75	40	Y	Linear
25	0.6	0.3	25	30	X	Honeycomb
26	0.6	0.3	50	40	Y	Rectilinear
27	0.6	0.3	75	20	X45°	Linear

Table 4 Parameters set constant for the additive manufacturing process

Parameter	Value	Parameter	Value
Contour width	1.2 mm	*Brim*	5 mm
Solid upper layers width	1.2 mm	*Overlap*/contour intersection	15%
Solid lower layers width	1.2 mm	Support material	No
Extra contour	Required	Space between filaments	1.5 mm
Combine filling every	2 layers	*Raft* (base layer)	No
Flow ratios	1	Speed trips in vacuum	130 mm/s
Extruder parameters			
Parameter	Value	Parameter	Value
Retraction length	2 mm	Extra length when reprinting	0 mm
Raise in Z	0 mm	Minimum distance for shrinkage	2 mm
Speed retraction	40 mm/s		

Experiments were performed with a Zwick Roell ProLine TABLE-TOP Z020 universal testing machine (Figure 4). Force data is measured through a 500-N load cell connected to a Spider8 DAQ device. An HD camera is also synchronized to the data acquisition system with the aid of a switch-controlled flashing light to record the state of the specimen at 60 Hz. This will allow to pair displacement and force data to build the stress-strain curve for each test. Data is processed by TestExpert software.

The ASTM standard outlines two different test procedures, as referenced by Travieso-Rodriguez *et al.* (2019). In this case, the B-type test was selected, as the specimens show large deflections. For that reason, the test was performed with a speed of 19 mm/min and was ended either when the specimen broke or when it showed a deflection of 10.9 mm.

2.5 Processing of results

To analyze the mechanical properties of each specimen, results must be processed after each test. This processing consists of tracking the photograms acquired by the camera to compute deformation, and secondly, calculating the strength data of the load cell to construct the stress-strain curve for each case. For

Figure 3 Four-point bending test diagram

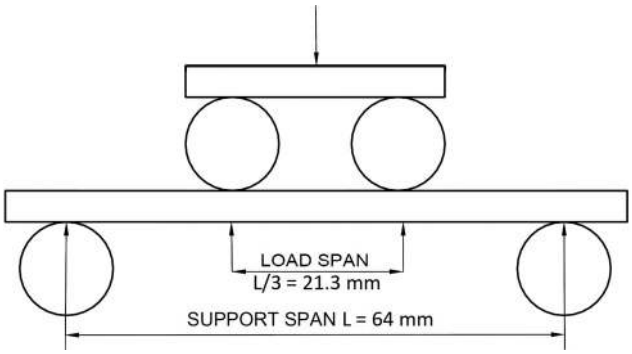

Figure 4 Zwick Roell test machine Z020 and mounting block diagram

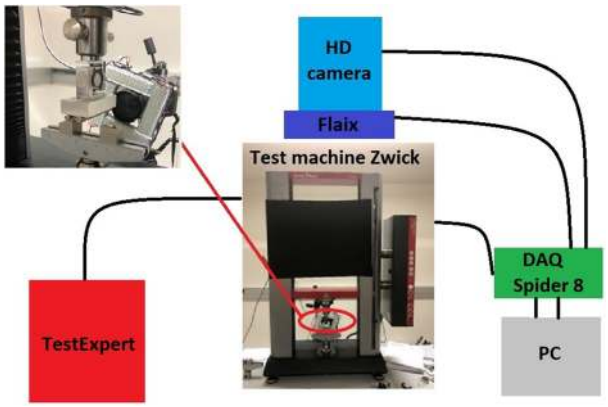

the first process, the HD video obtained for each test must be separated into frames. The camera captured 60 frames per second and, as the average test duration is 50 s, the average number of frames per video file is 3000. A MATLAB script is used to generate a mesh in the initial frame of the specimen. This mesh consists of a straight line divided into 50 points for the outer fiber and two rectangular meshes for the support rollers. The linear mesh must occupy approximately the space from the center to the center of the two rollers, as it is where the maximum deflection will occur. Video processing is also performed with a MATLAB script, starting from the first frame that contains the mesh. As the frames progress, the marked pixels are tracked and the deflection is calculated at each point, as the roller mesh is fixed and can therefore determine the difference between the initial and the final position. The results are recorded in a displacement matrix on the x-axis and in another one on the y-axis. Once the deflection information has been obtained, the displacement values of the markers will be transformed into actual deformations of the external fiber. The script is also able to detect the end of the test, either because there has been a breakage of fibers or because the rollers have reached their maximum point and are retracted.

From the strain-stress curve obtained from the test, four parameters characterizing the bending behavior of all specimens the are computed and subjected to ANOVA to evaluate the influence of factors included in the DOE. To obtain them they have been defined as follows:

1 Young's modulus (E). It is calculated based on the iteration of the points that show less error in the elastic zone. Once defined, the slope that is created between the three is calculated.
2 Elastic Limit ($Rp_{0.2}$). Straight line parallel to Young's Modulus displaced by 0.2%.
3 Maximum stress (σ_{max}). Maximum absolute value of stress observed in the graph.
4 Maximum deformation (Ɛ). Highest deformation value observed in the graph, either at break point or at 10.9-mm deflection, as describes the standard.

3. Result discussion

The summary of the mechanical properties calculated for each type of specimen is included in Table 5. These results were subjected to ANOVA tests to assess the statistical influence of each factor on their values. For each factor and mechanical property, the p-values are calculated and compared to a significance level of 5%. Then, the factors that can be identified as influential on the response are identified. The analysis includes the second-order interactions between parameters specified in the second section.

3.1 Young's modulus

The mean effects graph resulting from the ANOVA represented in Figure 5(A) shows that only layer height and

Table 5 Average results and standard deviations of the material properties

	E (GPa)	SD	$Rp_{0.2}$ (MPa)	SD	σ_{max} (MPa)	SD	ε (%)	SD
1	2.236	0.08	45.99	1.80	55.19	1.92	5.24	0.10
2	2.495	0.07	51.95	1.27	58.98	1.31	5.26	0.19
3	2.251	0.06	45.37	0.06	58.23	1.47	5.17	0.61
4	2.130	0.13	44.85	0.13	50.66	0.98	5.41	0.12
5	2.084	0.09	41.77	0.09	51.84	1.01	5.41	0.12
6	2.225	0.03	49.05	0.03	61.34	0.27	5.22	0.10
7	1.182	0.29	9.41	0.29	10.14	1.94	1.22	0.16
8	1.888	0.07	15.18	0.07	16.16	3.47	0.96	0.16
9	1.908	0.08	44.02	0.08	54.97	1.36	5.73	0.13
10	1.889	0.33	38.79	8.17	46.50	10.01	4.36	0.59
11	2.217	0.07	43.97	1.25	56.42	1.17	4.87	0.35
12	2.557	0.03	54.26	0.43	66.24	0.67	5.42	0.07
13	2.191	0.09	46.79	0.85	55.99	0.81	5.19	0.26
14	2.220	0.08	47.95	0.39	55.50	1.39	5.36	0.89
15	2.189	0.07	48.58	1.71	61.86	1.95	5.58	0.10
16	2.050	0.11	42.72	0.93	50.06	0.88	5.64	0.23
17	1.978	0.13	40.79	1.41	51.57	2.21	5.28	0.14
18	1.850	0.11	40.87	0.27	54.11	1.14	5.34	0.33
19	2.474	0.14	53.92	1.56	62.25	3.24	5.05	0.22
20	2.359	0.09	49.94	1.07	57.87	1.39	4.25	0.20
21	2.004	0.33	47.54	5.79	60.83	8.04	5.41	0.49
22	2.175	0.05	46.35	1.20	56.61	1.84	5.11	0.36
23	2.007	0.05	46.60	0.96	58.90	1.22	5.78	0.21
24	2.538	0.15	51.86	1.09	66.08	1.09	5.19	0.11
25	2.058	0.09	47.42	1.28	58.08	1.67	5.24	0.16
26	2.475	0.15	48.87	0.94	58.96	0.95	5.04	0.17
27	1.973	0.11	46.88	1.42	60.78	1.25	5.48	0.19

Figure 5 Young's modulus (E)

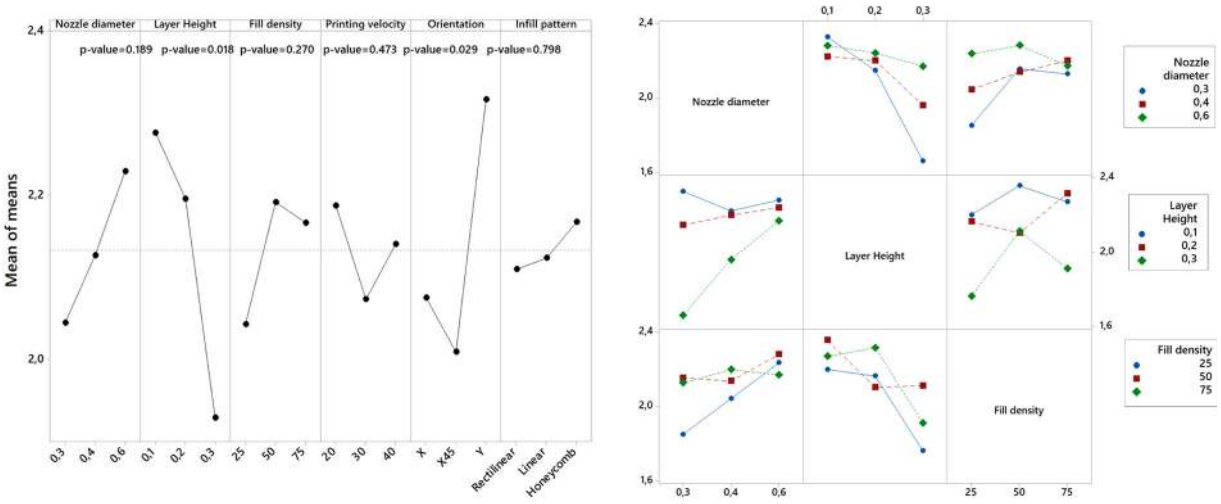

Notes: (a) Main effect graph for means; (b) interaction graphs for means

raster orientation are influential on the Young's modulus. The most significant change occurs when then layer height is decreased from 0.2 to 0.3 mm, what shows that choosing a very reduced layer height results in more rigid pieces. Indeed, this means greater compactness of the material within the piece, and therefore fibers are more effectively restricted to be elastically deformed, as explain Sood *et al.* (2012). The Y orientation also evidences higher rigidity of the workpiece. This can be explained by the fact that, although the longitudinal rasters work equally in all of them, the transverse ones work as compressed pillars in the case of the Y orientation with maximum inertia. These pillars also act as bracings for the longitudinal beams subjected to bending stress, as already observed Gurrala and Regalla (2014). On the other hand, it can be said that there is an interaction between the nozzle diameter and the layer height [Figure 5(B)], as there is an abrupt fall of the Young's module value when the 0.3-mm nozzle is combined with a 0.3-mm layer height. Indeed, this combination leads to a lack of cohesion between fibers of the stacked layers, along with a higher macroscopic porosity to liberates the movement of the fibers. This was already observed by Gómez-Gras *et al.* (2018).

3.2 Elastic limit

The statistical analysis evidences that layer height is still the most influential parameter to define the elastic limit, and that, again, increasing it from 0.2 to 0.3 mm causes an almost vertical drop in that value [Figure 6(A)]. In this case, the

Figure 6 Elastic limit ($Rp_{0,2}$)

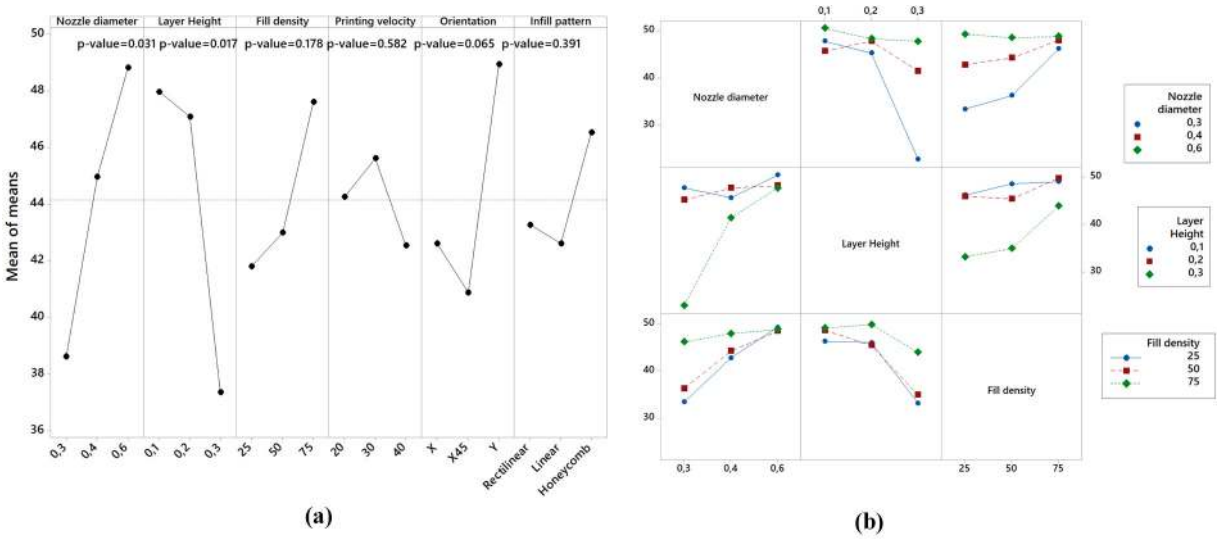

Notes: (a) Main effect graph for means; (b) interaction graphs for means

highest nozzle diameter does derive in a higher value for this mechanical property. The orientation's p-value is in the boundary between influential or not, but in any case, it seems that in average, the Y orientation is again the best to achieve the maximum elastic limit. Finally, the interaction between the nozzle diameter and the layer height evidences that using an excessive layer height with regards to the nozzle diameter has a negative effect in the elastic limit [Figure 6(B)]. The described effects can be interpreted in terms of how the material is added and distributed inside the specimens. Low layer heights and bigger nozzle diameters influence positively the elastic limit because they lead to less porous workpieces, where the rasters have more contact surface between them due to higher neck growth rates. Also, the transverse fibers in the Y orientation, oriented as pillars with regards to the bending axis, reinforce that direction, making the specimen more resistant in overall.

3.3 Maximum stress

Figure 7(A) shows the results of the variance analysis for the maximum stress. This property, unlike the two previous ones, refers to the behavior in the plastic domain, and therefore, shows different influence of factors. Layer height and nozzle diameter are influential in this case, as in the previous ones, but the orientation has ceased to influence the response. A lower layer height and higher nozzle diameter favor the increase of the maximum strength, being unadvised the combination of 0.3 mm value for both of them.

On the other hand, the fill density seems to have recovered here relevance, as it is shown that a higher infill percentage has a positive effect in the value of maximum strength that the material is able to bear. The change in the trend of how factors influence the response can be originated in the fact that, in this point, the workpiece is totally deformed, so that the fibers below the neutral fiber are subjected to tensile stress and the ones above it are compressed. The degree of deformation is such that in the section of the specimen subjected to tensile, the infill percentage gains relevance to bear the external load, as is clearly shown in Zandi *et al.* (2020a).

3.4 Maximum elongation

The last property to be analyzed is the maximum elongation. This is a more complex parameter to analyze by means of DOE, as the majority of specimens reached the maximum deformation set by the test without breaking. This has clearly interfered in the results, as all ANOVA tests show that no factor is influential on the response. This is not because mean values are similar, as Basik *et al.* (2010) also remark, but that the error associated to the statistical test is too high. For this reason, these results must be taken into account slightly (Figure 8).

In overall, the infill pattern was not statistically significant in any of the studied responses. This could contradict what some authors state at the (Domingo-Espín *et al.*, 2015), but the reason behind this could be that the reduced size of the specimens, and the prevalent effect of the solid perimeter conceal the influence of the infill. The fact that all three tested patters are at the end of the day a two-dimensional pattern could also soften its overall effect. Also, none of the three printing velocities studied were significant in terms of the mechanical properties studied. This result could be expected for two reasons. First, again the reduced size of the specimens makes that the time to generate each layer is almost the same one, what homogenizes the effect of thermal history, and no preferential effect in layer welding is observed. Secondly, the range of printing velocities is limited to a relatively small range of values, as too high values would prevent the layers to appropriately weld.

3.5 Summary

Figure 9 provides an overview of the results presented above. It shows that the nozzle diameter and the layer height are the two most relevant parameters to be controlled to maximize all mechanical properties, as found in PLA (Travieso-Rodriguez *et al.*, 2019) and

Figure 7 Maximum stress (σ_{max})

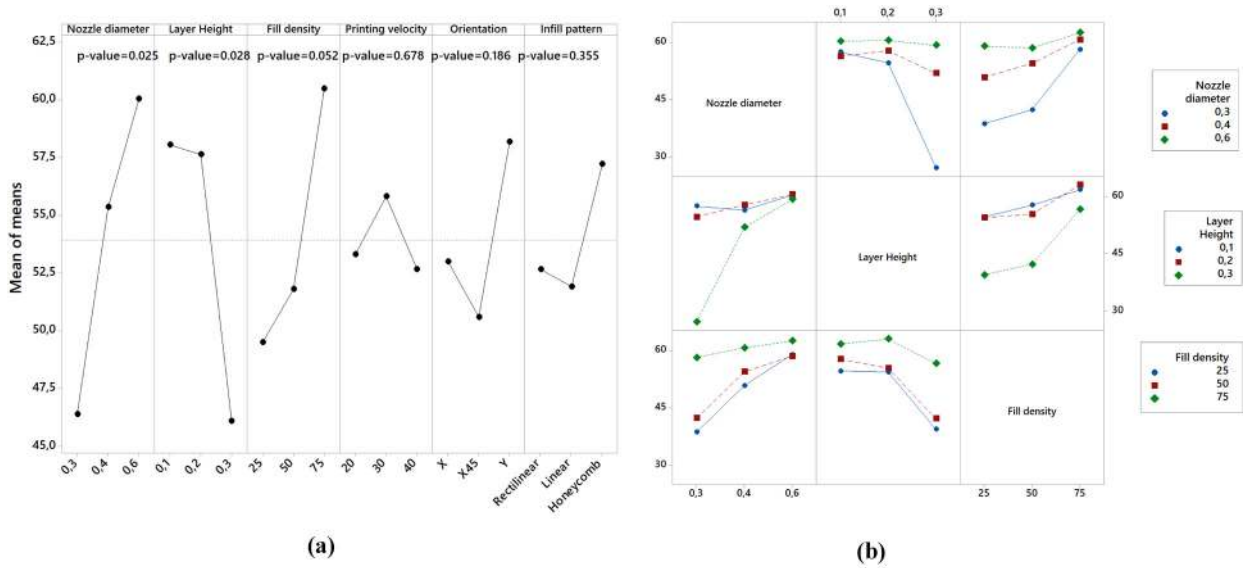

Notes: (a) Main effect graph for means; (b) interaction graphs for means

Figure 8 Maximum Elongation (ε)

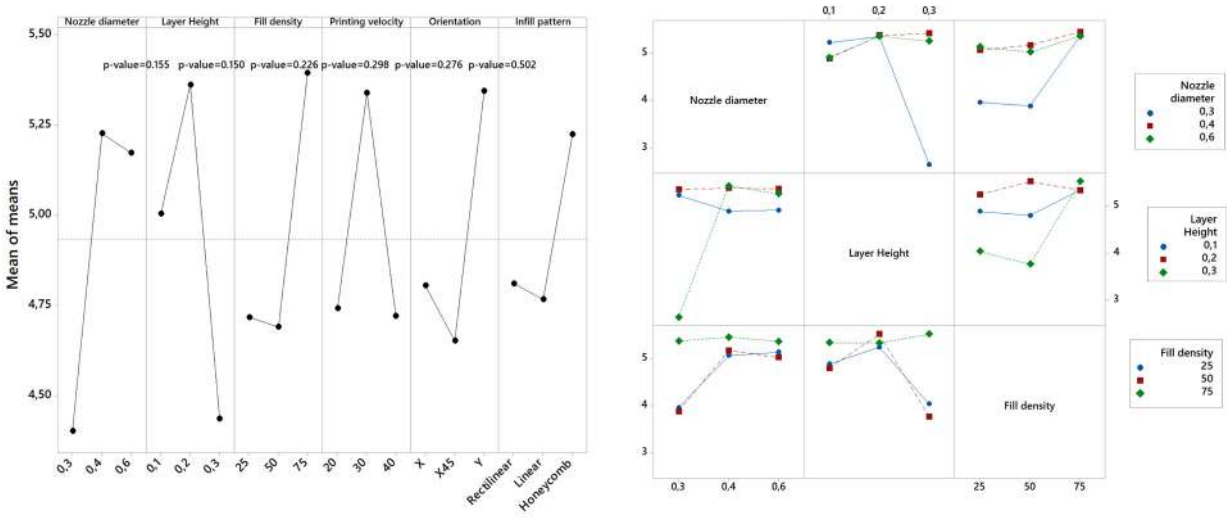

Notes: (a) Main effect graph for means; (b) interaction graphs for means

Figure 9 Summary of the significance of factors on all analyzed responses. Green: correlated. Yellow: slightly correlated. Red. Non-correlated

Parameter	Response			
	Elastic characteristics		Plastic characteristics	
	Young's modulus (E)	Elastic limit ($Rp_{0,2}$)	Maximum stress (σ_{max})	Maximum deformation (ε)
Layer Height				
Nozzle diameter				
Orientation				
Infill density				
Printing velocity				
Infill				

Notes: Green: correlated; yellow: slightly correlated; red: Non-correlated

Timberfill (Zandi *et al.*, 2020b), but also, that when the workpieces work in the plastic zone, the infill should be maximized, as it gains relevance as the specimens are more deformed.

Table 6 shows the best parameter values obtained that maximize the rigidity and the bending resistance within the scope of the experiment. The following criteria were applied: the value of the parameter that maximizes the response in the case of significant parameters is chosen, when the parameter is not significant but it was for another property, it maintains the previous value, and in the case of the non-significant parameter, its value is chosen according to economic, time or quality criteria.

3.6 Optical inspection of specimens

As an individual parameter, layer height has proved to be a statistically significant parameter, delivering the best responses when it is 0.1 mm. The best results have always been obtained for this value. This is not surprising, as for lower layer heights,

Table 6 Combination of best parameters to improve the flexural resistance of ABS

Parameter	Valor
Nozzle diameter	0.6 mm
Layer Height	0.1 mm
Infill density	75%
Printing velocity	30 mm/s*
Orientation	Y-axis
Infill	Honeycomb**

Notes: *For the printing speed, the central level is recommended, as it is the compromise between print quality and total printing time. If one of the two concepts were to become more important, the value could be increased to the top level or decreased to the lower one without significantly affecting mechanical resistance. **For the pattern, Honeycomb is recommended as it has the highest printing speeds

there is less empty space between filaments, resulting in a higher compactness that generates a more solid piece where filaments are better welded and neck growth is more effective, as already described Bellehumeur *et al.* (2004). The effect is similar for high values of the nozzle diameter, due to the same reasons: it all comes down to favoring neck growth between layers. To confirm it, pictures of the cross section was taken with a MOTIC SMZ-168 microscopy. Figure 10(A) represents the section combining 0.1 mm layer height and a 0.6-mm nozzle diameter. A combination of both values lead to ovoidal-section filaments with maximum area of contact, which favors neck growth, and increases the cohesive forces between layers. Also, voids between filaments are almost inconspicuous, making the section highly compact.

Much on the contrary, the combination of 0.3-mm nozzle diameter and 0.3-mm layer height shows voids [Figure 10(B)], and weak contact between deposited filaments is observed. Indeed, deposited fibers have cylindrical cross-section, producing a detrimental contact between the filaments and causing an extremely poor neck growth. This explains the fall in all responses when the interaction between these two was analyzed above.

Density has only reached the threshold of significance in the maximum stress. This result is highly unexpected, at sight of the conclusions of other authors such as Torres *et al.* (2015). However, it is important to note that the actual cross section of the tested specimens is 7.6 x 1.8 mm. From that section, most of it is composed of an external perimeter, which had to be fixed at 1.2 mm so that it could be achievable with all layer heights. Consequently, most of the bearing strength of the section is accounted to this perimeter, and its effect clearly conceals the effect of the infill density. In other words, the material inside the perimeter is not needed to achieve good strength. This is perfectly depicted by Figures 11(A) and (B), that show pieces with 25% density and two different infills. The only reason why density is influential in the maximum stress value is that the infill becomes relevant at high levels of deformation, when the original fibers are completely deformed.

3.7 Fractography analysis

In addition to assessing the effects of each of the parameters separately, other conclusions can also be drawn from the test. Figure 12 shows ductile fractures in the studied pieces, at sight

Figure 10 Cross-section image of singular specimens

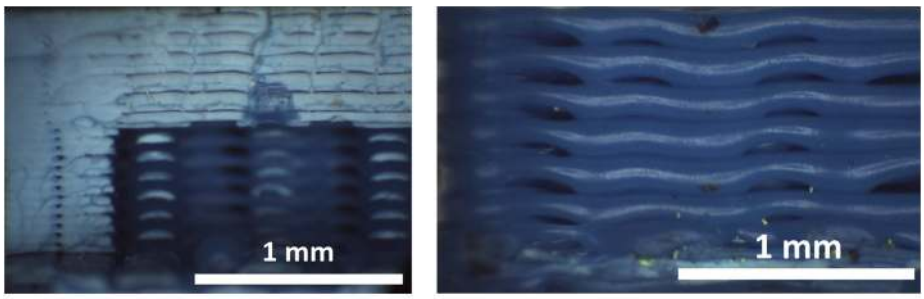

Notes: (a) 0.6 mm nozzle diameter – 0.1 mm layer height - 50% fill density – 20 mm/s printing velocity – 45° orientation and rectilinear infill pattern; (b) 0.3 mm Nozzle diameter – 0.3 mm layer height – 25% fill density – 40mm/s printing velocity – 45° orientation and rectilinear infill pattern

Figure 11 Cross-section image of singular specimens

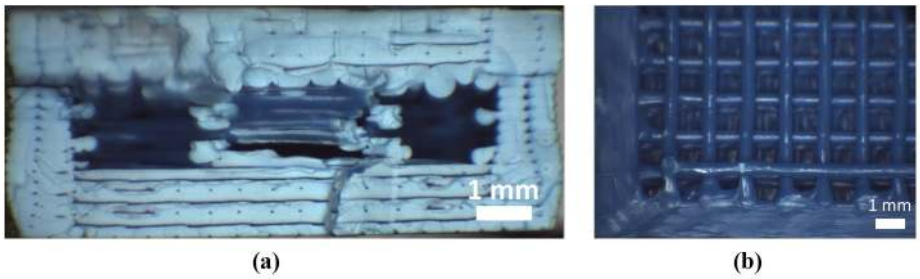

Notes: (a) 0.6 mm nozzle diameter – 0.1 mm layer height - 50% fill density – 20 mm/s printing velocity – 45° orientation and rectilinear infill pattern; (b) 0.3 mm Nozzle diameter – 0.3 mm layer height – 25% fill density – 40mm/s printing velocity – 45° orientation and rectilinear infill pattern

Figure 12 Microscopy MOTIC SMZ-168 picture

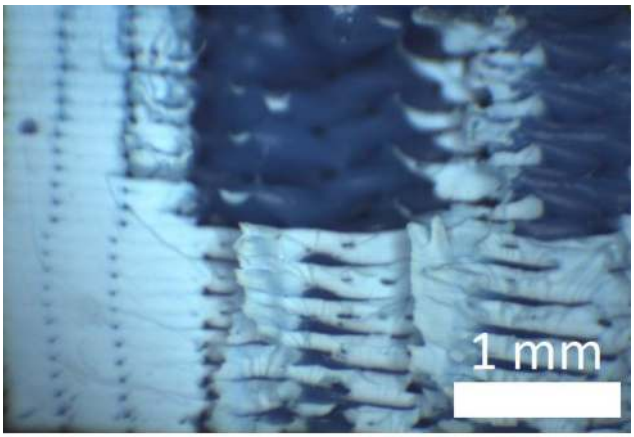

Notes: Specimen printed with 0.4 mm nozzle diameter – 0.1 mm layer height - 50% fill density – 40 mm/s printing speed – 45° orientation and Honeycomb infill pattern

of the white color of the fibers during plastification and through the deformation they have undergone, as also shown by Domingo-Espin *et al.* (2019). The fibers have also become deformed, adopting an elliptical shape. It is also interesting to notice how strong adhesion occurs between layers, where two are joined together and between two layers that are joined together and the next two there is a space. This is because the printing process does not always follow the same path, rather it completes the first trajectory in one direction and the second in the opposite direction, and so on.

3.8 Comparison of ABS, PLA and Timberfill

It is interesting to make a comparison of the obtained results for ABS and two other materials that are also used to manufacture pieces through FFF, taking advantage of the fact that all materials were studied through the same experimental design. These are the polylactic acid (PLA), a polymer made up of molecules of lactic acid with properties that are similar to polyethylene, and a composite of itself called Timberfill, with is composed of PLA reinforced with round 8% wood particles. Adding wood to the PLA makes it possible to obtain pieces with a wooden look, though the properties of the material vary considerably.

PLA and Timberfill were respectively studied with the same experimental design by Travieso-Rodriguez *et al.* (2019) and Zandi *et al.* (2020b) as those described for the ABS in this paper. A summary of those results are included in Table 7. The chosen parameters are almost the same for the three materials, except for the printing velocity parameter, that should be reduced to maximize bending strength in the case and PLA. Also, in the case of Timberfill, higher values of the nozzle diameter are recommended to facilitate the flow of wood particles through it.

To contextualize the results, it is also useful to compare the maximum values obtained for each of the response factors for all the materials studied as in Table 8. These results show that in absolute terms PLA behaves better than ABS and Timberfill. It is more rigid, has a higher elastic limit, holds superior maximum stress and the elongation it can achieve is greater. For that reason, ABS should be recommended only if the workpiece is to withstand higher in-service temperatures, as its glass transition temperature is higher.

Regardless of the maximum values obtained for each property on the three materials, a case-by-case comparison can be made between the specimens manufactured with the same parameters. Table 9 shows two different kind of specimens manufactured in the same conditions the properties obtained. For specimens in Line 1, PLA achieves a worst elastic behavior than ABS, with lower rigidity. However, it is better in terms of the maximum stress and the maximum deflection reached, showing the most ductile behavior of all three materials. This was also observed by Efstathiadis *et al.* (2018). This is an indicator that fewer static failure can be expected to occur with PLA than with ABS. For specimens in Line 2, the situation is

Table 7 Optimal parameters found in bending tests for ABS, PLA (Travieso-Rodriguez *et al.*, 2019) and Timberfill (Zandi *et al.*, 2019)

	Material/Chosen level		
	ABS	PLA	Timberfill
Layer height (mm)	0.1	0.1	0.2
Nozzle diameter (mm)	0.6	0.6	0.7
Fill density (%)	75	75	75
Printing velocity (mm/s)	40	20	35
Layer orientation	Y	Y	Y
Infill pattern	Honeycomb	Honeycomb	Honeycomb

Table 8 Maximum values obtained in bending tests for ABS, PLA (Travieso-Rodriguez *et al.*, 2019) and Timberfill (Zandi *et al.*, 2019)

	Material		
	ABS	PLA	Timberfill
Young's Modulus (GPa)	2.55	3.70	2.41
Elastic Limit (MPa)	54.26	90.8	38.06
Maximum Stress (MPa)	66.24	109.5	47.26
Maximum Deformation (%)	5.78	6.21	5.34

Table 9 Comparative results of four-point bending tests of representative specimens. Nozzle diameter: 0.6 mm and honeycomb infill pattern

		PLA				ABS				Timberfill			
Fill density (%)	Layer height (mm)	E (GPa)	$Rp_{0.2}$ (MPa)	σ_{max} (MPa)	ε (%)	E (GPa)	$Rp_{0.2}$ (MPa)	σ_{max} (MPa)	ε (%)	E (GPa)	$Rp_{0.2}$ (MPa)	σ_{max} (MPa)	ε (%)
25	0.3	1.92	44.5	61.7	6.10	2.06	47.42	58.08	5.24	1.82	36.58	34.94	3.80
50	0.2	2.85	63.4	86.4	5.36	2.23	46.54	59.02	5.89	2.12	31.83	39.76	4.35

completely the opposite. It means that increasing the infill density and reducing the layer height, the PLA specimens show higher sensitivity to mechanical properties enhancement, except for the maximum deflection. This situation where PLA was superior to ABS, for some printing conditions, was also observed by Rodríguez-Panes *et al.* (2018). Tymrak *et al.* (2014), had already observed that there can be great variability in the properties of parts manufactured in PLA, depending on how they have been printed, a fact that is evidenced in this paragraph.

On the other hand, in both cases Timberfill specimens have worse mechanical properties than ABS and PLA, regardless of manufacturing conditions. This has been also observed in previous studies, comparing different stress states by Zandi *et al.* (2020a, 2020b). It means that in general, Timberfill performs worse than the other two, so its use should be questioned depending on the levels of mechanical stress expected. Despite being a relatively inexpensive, wood-looking, biodegradable material, it is not competitive against ABS and PLA. By contrast, parts made of ABS and PLA can have similar properties, depending on the parameters used for their manufacture. Clearly the advantage of PLA over ABS is that it is a biodegradable material that comes from abundant non-fossil resources in nature.

4. Conclusions

In this paper, experimental data regarding flexural behavior of ABS specimens has been collected and analyzed. Results show that the layer height and the nozzle diameter should be respectively decreased and increased to obtain the best results in terms of strength and rigidity of ABS parts. Also, the orientation is of high importance, so that parts that are expected to be subjected to bending loads should be manufactured so that their transverse filaments should be perpendicular to the bend turning axis (what was called Y orientation in this paper). It is also worth mentioning that the nozzle diameter and layer height have an important interaction between them, and should never have equal values to guarantee neck growth between filaments, and thus enough interlayer cohesion. At sight of these results, the layer height should be at most 75% of the nozzle diameter. Finally, ABS shows ductile behavior when processed through FFF and failure through bending.

In a second phase, these results were compared to others arising from a similar study with PLA and PLA–wood composite (Timberfill) specimens. It was proved that for certain manufacturing parameters, PLA present more rigidity than ABS when subjected to bending stress, although ABS can experience more deflection before fracture, and for certain conditions the opposite happens. Finally, the use of Timberfill should be reserved for purely esthetic purposes, as its properties are lower than PLA and ABS in all tested cases.

AQ: 8

References

Andrzejewska, A., Pejkowski, L. and Topoliński, T. (2019), "Tensile and fatigue behavior of additive manufactured polylactide", *3D Printing and Additive Manufacturing*, Vol. 6 No. 5.

Aydin, L. and Kucuk, S. (2018), "A method for more accurate FEA results on a medical device developed by 3D technologies", *Polymers for Advanced Technologies*, Vol. 29 No. 8, pp. 2281-2286.

Bagsik, A., Schöppner, V. and Klemp, E. (2010), "FDM part quality manufactured with ultem 9085", Proceedings of the 14th international scientific conference on polymeric materials, 2010, Halle, pp. 307-315.

Bellehumeur, C.T., Li, L., Sun, Q. and Gu, P. (2004), "Modeling of bond formation between polymer filaments in the fused deposition modeling process", *Journal of Manufacturing Processes*, Vol. 6 No. 2, pp. 170-178.

Belouettar, S., Abbadi, A., Azari, Z., Belouettar, R. and Freres, P. (2009), "Experimental investigation of static and fatigue behaviour of composites honeycomb materials using four point bending tests", *Composite Structures*, Vol. 87 No. 3, pp. 265-273.

Domingo-Espin, M., Puigoriol-Forcada, J.M., Garcia-Granada, A.A., Llumà, J., Borros, S. and Reyes, G. (2015), "Mechanical property characterization and simulation of fused deposition modeling polycarbonate parts", *Materials & Design*, Vol. 83, pp. 670-677.

Domingo-Espin, M., Travieso-Rodriguez, J.A., Jerez-Mesa, R. and Lluma-Fuentes, J. (2018), "Fatigue performance of ABS specimens obtained by fused filament fabrication", *Materials*, Vol. 11 No. 12, p. 2521.

Efstathiadis, A., Koidis, C., Tzetzis, D. and Kyratsis, P. (2018), "Comparative study and analysis on the mechanical properties of 3d printed surgical instrument for in-space applications", *Academic Journal of Manufacturing Engineering*, Vol. 16 No. 4.

Garg, A., Bhattacharya, A. and Batish, A. (2017), "Chemical vapor treatment of ABS parts built by FDM: analysis of surface finish and mechanical strength", *The International Journal of Advanced Manufacturing Technology*, Vol. 89 Nos 5/8, pp. 2175-2191.

Gibson, I., Rosen, D. and Stucker, B. (2010), *Additive Manufacturing Technologies 3D Printing, Rapid Prototyping, and Direct Digital Manufacturing*, Springer, New York, NY.

Gomez-Gras, G., Jerez-Mesa, R., Travieso-Rodriguez, J.A. and Lluma-Fuentes, J. (2018), "Fatigue performance of fused filament fabrication PLA specimens", *Materials & Design*, Vol. 140, pp. 278-285.

Guo, N. and Leu, M.C. (2013), "Additive manufacturing: technology, applications and research needs", *Frontiers of Mechanical Engineering*, Vol. 8 No. 3, pp. 215-243.

Gurrala, P.K. and Regalla, S.P. (2012), "Prediction of neck growth due to inter and Intra-Layer bonding for high strength parts in additive manufacturing (AM)", *4th International & 25th All India Manufacturing Technology, Design & Research*, Jadavpur University, Kolkata.

Gurrala, P.K. and Regalla, S.P. (2014), "Part strength evolution with bonding between filaments in fused deposition modelling: this paper studies how coalescence of filaments contributes to the strength of final FDM part", *Virtual and Physical Prototyping*, Vol. 9 No. 3, pp. 141-149.

Jerez-Mesa, R., Gomez-Gras, G., Travieso-Rodriguez, J.A. and Garcia-Plana, V. (2018), "A comparative study of the thermal behavior of three different 3D printer liquefiers", *Mechatronics*, Vol. 56, pp. 297-305.

Liu, Z., Lei, Q. and Xing, S. (2019), "Mechanical characteristics of wood, ceramic, metal and carbon fiber-based PLA composites fabricated by FDM", *Journal of Materials Research and Technology*, Vol. 8 No. 5, pp. 3741-3751.

Peker, A., Aydin, L., Kucuk, S., Ozkoc, G., Cetinarslan, B., Canturk, Z. and Selek, A. (2020), "Additive manufacturing and biomechanical validation of a patient-specific diabetic insole", *Polymers for Advanced Technologies*, Vol. 31Issue No. 5, pp. 988-996.

Pîrjan, A. and Petroşanu, D.M. (2013), "The impact of 3D printing technology on the society and economy", *Journal of Information Systems & Operations Management*, Vol. 7 No. 2, pp. 360-370.

Puigoriol-Forcada, J.M., Alsina, A., Salazar-Martín, A.G., Gomez-Gras, G. and Pérez, M.A. (2018), "Flexural fatigue properties of polycarbonate fused-deposition modelling specimens", *Materials & Design*, Vol. 155, pp. 414-421.

Rodríguez-Panes, A., Claver, J. and Camacho, A.M. (2018), "The influence of manufacturing parameters on the mechanical behaviour of PLA and ABS pieces manufactured by FDM: a comparative analysis", *Materials*, Vol. 11 No. 8, p. 1333.

Sood, A.K., Ohdar, R.K. and Mahapatra, S.S. (2010), "Parametric appraisal of mechanical property of fused deposition modelling processed parts", *Materials & Design*, Vol. 31 No. 1, pp. 287-295.

Sood, A.K., Ohdar, R.K. and Mahapatra, S.S. (2012), "Experimental investigation and empirical modelling of FDM process for compressive strength improvement", *Journal of Advanced Research*, Vol. 3 No. 1, pp. 81-90.

Sun, Q., Rizvi, G.M., Bellehumeur, C.T. and Gu, P. (2008), "Effect of processing conditions on the bonding quality of FDM polymer filaments", *Rapid Prototyping Journal*, Vol. 14 No. 2, pp. 72-80.

Travieso-Rodriguez, J.A., Zandi, M.D., Jerez-Mesa, R. and Lluma-Fuentes, J. (2020), "Fatigue behavior of PLA-wood composite manufactured by fused filament fabrication", *Journal of Materials Research and Technology*, Vol. 9 No. 4, doi: 10.1016/j.jmrt.2020.06.003.

Travieso-Rodriguez, J.A., Jerez-Mesa, R., Llumà, J., Traver-Ramos, O., Gomez-Gras, G. and Roa Rovira, J.J. (2019), "Mechanical properties of 3D-printing polylactic acid parts subjected to bending stress and fatigue testing", *Materials*, Vol. 12 No. 23, p. 3859.

Tymrak, B.M., Kreiger, M. and Pearce, J.M. (2014), "Mechanical properties of components fabricated with open-source 3-D printers under realistic environmental conditions2", *Materials & Design*, Vol. 58, pp. 242-246.

Wang, T.M., Xi, J.T. and Jin, Y. (2007), "A model research for prototype warp deformation in the FDM process", *The International Journal of Advanced Manufacturing Technology*, Vol. 33 Nos 11/12, pp. 1087-1096.

Zandi, M.D., Jerez-Mesa, R., Llumà, J., Jorba-Peiro, J. and Travieso-Rodriguez, J.A. (2020a), "Comparative study of tensile properties between fused filament fabricated and injection-molded Wood-PLA composite parts", *The International Journal of Advanced Manufacturing Technology*, Vol. 108 Nos 5/6, doi: 10.1007/s00170-020-05522-4.

Zandi, M.D., Jerez-Mesa, R., Lluma-Fuentes, J., Roa, J.J. and Travieso-Rodriguez, J.A. (2020b), "Experimental analysis of manufacturing parameters' effect on the flexural properties of wood-PLA composite parts built through FFF", *The International Journal of Advanced Manufacturing Technology*, Vol. 106 Nos 9/10, pp. 3985-3998, doi: 10.1007/s00170-019-04907-4.

Further reading

ASTM D6272–17 (2017), ASTM D6272–17 Standard Test Method for Flexural Properties of Unreinforced and Reinforced Plastics and Electrical Insulating Materials by Four-Point Bending. Ed, ASTM International, West Conshohocken, PA.

Slic3r User's Manual (2020), available at: https://manual.slic3r.org/intro/getting-support, Last consulted on 14 May 2020.

Olivier, D., Travieso-Rodriguez, J.A., Borros, S., Reyes, G. and Jerez-Mesa, R. (2017), "Influence of building orientation on the flexural strength of laminated object manufacturing specimens", *Journal of Mechanical Science and Technology*, Vol. 31 No. 1, pp. 133-139.

Wohlers, T. and Gornet, T. (2016), "History of additive manufacturing", *Wohlers Report*, Wohler Associates, Fort Collins, CO.

Corresponding author

R. Jerez-Mesa can be contacted at: ramon.jerez@uvic.cat